AD-A134 257 CRITICAL DYNAMICS FOR CONTINUOUS RAPID SOLIDIFICATION PROCESSING(U) GTE LABS INC WALTHAM MA R P ADLER ET AL. SEP 83 TR-83-815.1 N00014-82-C-0434 1/1

UNCLASSIFIED F/G 11/6 NL

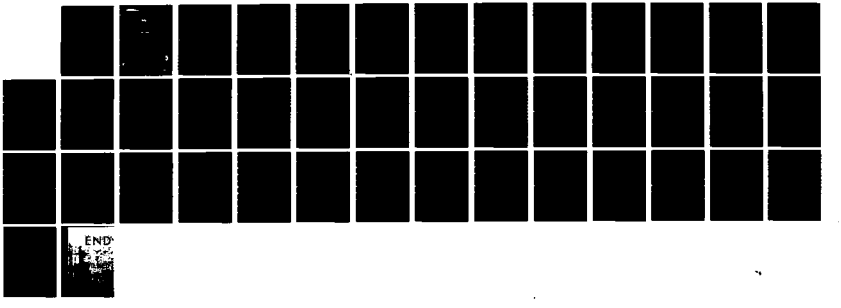

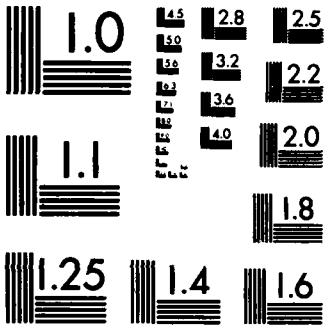

MICROCOPY RESOLUTION TEST CHART
NATIONAL BUREAU OF STANDARDS-1963-A

[redacted]

Research &
Development

TR 83-815.1

AD-A134257

Critical Dynamics for Continuous Rapid Solidification Processing

Prepared for:

Office of Naval Research
800 North Quincy Street
Arlington, VA 22217

by

R.P.I. Adler
S.C. Hsu

September 1983

DTIC FILE COPY

DTIC
ELECTE
NOV 1 1983
S D
A

GTE Laboratories Incorporated
40 Sylvan Road
Waltham, MA 02254

GTE

REPORT DOCUMENTATION PAGE

READ INSTRUCTIONS BEFORE COMPLETING FORM

1. REPORT NUMBER	2. GOVT ACCESSION NO. AD-A134257 / 3. RECIPIENT'S CATALOG NUMBER
4. TITLE (and Subtitle) Critical Dynamics for Continuous Rapid Solidification Processing	5. TYPE OF REPORT & PERIOD COVERED Annual Report for Period 6/82 - 7/83
	6. PERFORMING ORG. REPORT NUMBER TR83-815.1
7. AUTHOR(s) R.P.I Adler and S.C. Hsu	8. CONTRACT OR GRANT NUMBER(s) N0014-82-C-0434
9. PERFORMING ORGANIZATION NAME AND ADDRESS GTE Laboratories Incorporated 40 Sylvan Road Waltham, MA 02154	10. PROGRAM ELEMENT, PROJECT, TASK AREA & WORK UNIT NUMBERS NR 653-008
11. CONTROLLING OFFICE NAME AND ADDRESS Office of Naval Research 800 N. Quincy Street Arlington, VA 22217	12. REPORT DATE September 1983
	13. NUMBER OF PAGES 48
14. MONITORING AGENCY NAME & ADDRESS(if different from Controlling Office)	15. SECURITY CLASS. (of this report) Unclassified
	15a. DECLASSIFICATION/DOWNGRADING SCHEDULE

16. DISTRIBUTION STATEMENT (of this Report)

17. DISTRIBUTION STATEMENT (of the abstract entered in Block 20, if different from Report)

18. SUPPLEMENTARY NOTES

19. KEY WORDS (Continue on reverse side if necessary and identify by block number)

Rapid Solidification Processing, Dynamic Wetting, Transient Mass and Heat Transfer, Falling Droplet Simulation Testing, Melt Spinning, Melt Puddle Dynamics

20. ABSTRACT (Continue on reverse side if necessary and identify by block number)

DD FORM 1 JAN 73 1473

ABSTRACT

A standardized test procedure for simulating the dynamic wetting and solidification behavior during melt spinning was designed and is being used to generate pheonomenological information for various combinations of melt and substrate that would be desired. Real differences in dynamic wetting/solidification patterns have been found and suggested correlations with melt spinning performance have been proposed. Concurrently a set of melt spinning experiments are being conducted to provide complementary information about the interrelation of melt puddle/substrate dynamics with processability and product characteristics.

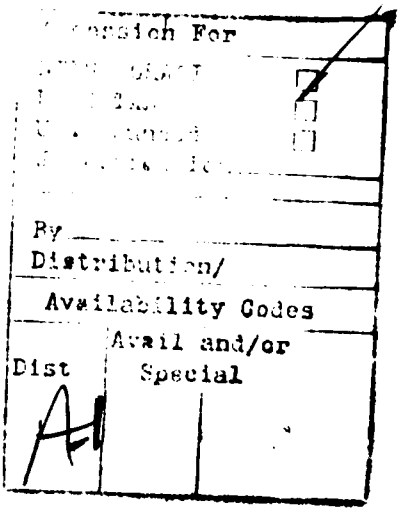

RE: Company Private, For Distribution Within GTE Only
Delete the above statement per Dr. David E. Polk, ONR/Code 430

TABLE OF CONTENTS

LIST OF TABLES

1. INTRODUCTION

As the potential advantages of using rapidly solidified materials to upgrade the performance of structural, propulsion, and electromagnetic systems become more apparent and applications more numerous, it will be more incumbent on materials suppliers to develop higher capacity processes for consistently producing a wide range of crystalline and amorphous alloys. In addition to efficiency and substantial capacity requirements for such rapid solidification processes, these operations must reliably generate high quality material with uniformly reproducible metallurgical and dimensional characteristics.

Melt spinning is one rapid solidification processing method that has already shown much commercial promise for a specific group of alloys. However, further progress to generate a more universal processing capability for a greater range of materials with additional improvement in the long term temporal stability (both thermal and mechanical) of equipment is also important. To do this a better understanding of many aspects of this continuous solidification phenomenon must be applied to the control and optimization of processing practices.

In its simplest elements, melt spinning involves: (1) the continuous metering of a liquid metal stream that spreads into a "stationary" puddle upon contact with a rotating, heat absorbing substrate; (2) the continuous growth of a thin, rapidly solidified film along the original melt/substrate interface; and (3) the concurrent transport of this continuous metal foil away from the puddle and the subsequent complete separation of that foil from the substrate. Thus for process continuity to be realized an appropriate balance between adequate melt/substrate contact and minimal foil/substrate adherence must be in effect.

However, since this form of rapid solidification can occur only with excellent heat transfer rates from the melt into the substrate, a primary objective of this dynamic wetting study will be to identify process and material factors that contribute to intimate melt/substrate contact. Prior classical wetting literature[1,2] already provides some indications regarding temporal changes in the fundamental nature of the respective interfaces that could occur when high surface energy liquids are involved. Either inherently or due to the higher operating temperatures, nascent liquid and solid surfaces can be quickly altered by reactions with each other and/or the ambient atmosphere. Such reactions generally produce oppositely directed effects on wettability. For the liquid (melt) the resultant reduction in surface tension promote wetting. For the solid (substrate) similar

decreases in surface energy (e.g., metal oxides typically have lower surface energies than the comparable parent metal surface) decrease wettability.

With melt spinning additional dynamic complexities influencing the spreading flow of the melt are introduced by: (1) the boundary layer of gas attached to the moving substrate surface; (2) the effectively steady state but geometrically transient coupled mass and heat flow patterns within the melt puddle; (3) the possible temporal changes in the thermal, morphological and chemical parameters of the substrate surface during operation; and (4) the systematically varying character of the dynamic wetting reaction around the puddle periphery (from an effectively advancing wetting phenomenon in the upstream region to a receeding one at the downstream portion due to resolved substrate shear and fluid momentum forces). These factors also affect the dimensional stability of the melt puddle, which in turn influences the quality and uniformity of the resultant melt spun products.

Clearly, a generalized approach to identify the significant combinations of materials and operating parameters that optimize the processing efficiency of melt spinning is desired without resorting to an extended experimental effort for each candidate alloy product. A simplified screening procedure that allows independent control or substitution of some potentially important material and phenomenological parameters has been designed for this program to simulate the essential melt spinning conditions. The present methodology has been able to discriminate between several classes of dynamic wetting and solidification behavior. The experimental portion of this study describes the equipment used and addresses the correlatability of the information generated with observed phenomenological characteristics of various materials during the melt spinning process.

2. RELATED WETTING/SPREADING STUDIES

The classical sessile drop representation[2] (Eq. 1) describes how the vectorial resolution of the surface tensions of the liquid (γ_l) and the solid (γ_s) surface with the interfacial tension of the liquid/solid interface (γ_{ls}) leads to the classification of wetting and nonwetting combinations.

$$\gamma_s = \gamma_l \cos\phi + \gamma_{ls} \quad (1)$$

Systems with contact angles ϕ (where ϕ is the supplement to the angle between the γ_s and γ_l vectors) greater than 90° are defined as nonwetting with larger ϕ values meaning even less relative wetting. Wetting systems are characterized by small contact angles ($\phi<90°$) with ϕ approaching zero for perfect wetting conditions. To promote wetting (e.g., minimize ϕ), steps to decrease γ_l and γ_{ls} in combination with relatively larger values of γ_s are needed.

Decreases in γ_{ls} can be attained by increasing the amount of reaction between the liquid and the solid (e.g., raise the contact temperature or increase the exposure time, especially if an intermetallic compound forms) or if there is some mutual solubility.[1,2] Selective solute additions to the melt can generally reduce γ_l but may also reduce γ_{ls} if that solute/solid combination forms an intermetallic compound or the additional solute is also mutually soluble in the solid[1-3] In contrast for a specific solid phase little can be done to raise its surface energy, but care must be taken to avoid all forms of surface impurities and contamination as well as atmosphere/solid reactions (especially oxides) since all these tend to decrease γ_s, inhibiting wetting.[1,2]

The relative roughness of the substrate surface can cause deviations from expected wetting behavior, with increases generally decreasing wettability. In practice the apparent contact angle of an advancing wetting front is greater than the equilibrium value,[4,5] thus any decrease in wetting is somewhat proportional to the degree of roughness. For sessile drops this effect can be reduced if the ambient temperature is raised or if some extraneous mechanical energy (e.g., ultrasonic vibrations) is imposed during testing.[4] The true area of surface contact can also be reduced by microtopological features. Thus for certain combinations of height and interspacing of surface asperities, the presence of high surface tension micromensci could drastically reduce the apparent substrate/liquid contact area.[6] Then for a solidifying melt that forms extensive micromensci on rougher substrates, the negative impact on the relative heat transfer rate

could reduce the effective solidification rate and the macrouniformity of the resultant microstructure.

The flow behavior of a liquid metal on a solid substrate is also affected by relative thermal effects. For static cases wetting is usually dominated by the surface tension forces between the liquid and the solid that are typically at the same temperature. Since small changes in temperature usually produce only a secondary change in the relative magnitudes of γ_s and γ_l, no substantial thermally related phenomenological changes are expected. The major factor then usually is any time dependent change in γ_s which may be affected by the degree and kinetics of the chemical interaction between the solid and the liquid. For dynamic cases such as melt spinning, liquid momentum forces produced by the continual introduction of melt into the puddle, as well as the substrate shearing and foil exiting effects, provide additional forces that favor spreading and these may be more important than surface tension forces. The mechanism of liquid flow[7] by the: (1) penetration, (2) overflow, or (c) mixing mode can affect the process as well as the product form and microstructure. The mode also depends on the relative "initial" temperatures of the melt and substrate, which are deliberately unequal but controllable parameters, to produce continuous, rapid solidification during the melt spinning operation. Since viscosity is an important parameter in fluid flow both temperature and alloy composition become important variables in controlling spreading flow. In fact alloy systems as well as specific compositions within each system are significant, because large variations in viscosity can occur. For example, some cases of eutectic alloys have lower viscosities than expected.[8] For increased spreading flow through thermal means, higher melt superheats[9-11] as well as hotter substrates[12] have been recommended. However, the minor effect of melt superheat, substrate surface roughness and ambient gas specie on gross product dimensions[13] indicates that for typical melt spinning conditions momentum forces are more important than thermally induced changes in melt viscosity, gas specie related changes in fluid flow and convective heat transfer characteristics, or variations in substrate microtopology.

A number of reports describe the effects of process variables on the dimensions of amorphous melt spun products,[13-15] as well as crystalline ones.[16,21] Since these values are in turn related to the melt puddle geometry and mass balance conditions, the fact that the foil thickness is inversely proportional to, and the foil width is independent of or weakly proportional to the tangential surface velocity of the rotating substrate, indicates that transverse fluid flow is considerably less than that in the primary direction. An illustrative example is based on an evaluation of

the transverse ribbon cross section as a function of liquid mass flow rate.[13] At very low rates a central mount is present; at intermediate values the profile is substantially flat; and at higher values parallel ridges develop along the edges of the free surface. Maximum transverse spreading occurs if the melt jet impinges at right angles to substrate surface at the point of contact where the impingement angle $\alpha = 90°$. α has been defined as the angle between tangential substrate surface velocity vector (at point of melt jet contact) and the jet flow axis in the plane defined by that velocity vector and the surface normal at the puddle contact site. At lesser angles of α the resolved momentum forces responsible for lateral spreading are proportional to $\sin\alpha$, so that foils tend to get thicker but narrower[13] as the jet impingement angle becomes shallower.

The dynamic effect of the gas boundary layer that is attached to the rotating substrate surface (except under high vacuum conditions) manifests itself in several forms. For instance, this flowing film can restrict melt puddle/substrate wetting as well as heat transfer, thus affecting product quality. Some fluid flow characteristics of this boundary layer can, however, be partially controlled by changing the composition and/or the pressure of these ambient gases and to a lesser extent by altering the surface finish of the substrate wheel. Edge serrations, especially for wider foils, are caused by gas boundary layer turbulences that interact with the melt puddle.[14,22] Such flow perturbations can be diminished by reducing the effective Reynolds number of the gas, and has already been demonstrated through the lowering of ambient operating pressures and the use of a lower molecular weight and higher kinematic viscosity gases (e.g., He).

The formation of a random or systematic pattern of voids on the contact surface of foils results from the entrapment of boundary layer gas between the substrate and the solidifying melt puddle. Slower wheel velocities[20] and finer (smoother) surface finishes[14] can reduce the frequency of these voids, but then the individual volumes of each void are frequently larger[23] than those in a more uniformly distributed set of voids such as can form from prenucleated pockets when a steel brush is used to continuously dress the wheel to a matte surface finish.[24] When a drastic reduction in the size and frequency of contact surface voids is warranted, the use of vacuum or low pressure He ambients can be most effective in improving the overall smoothness of contact surfaces.[20,25]

Considerations of the heat transfer component of this dynamic wetting/solidification phenomenon have been applied to the evaluation of product dimensions as well as the interpretation of the microstructural features of rapidly solidified materials as a function of relative solidification rate.

During the initial solidification phase or for very thin melts, increasing the interfacial heat transfer coefficient h to raise the solidification rate can be accomplished by using higher conductivity metallic substrates (where a gold plated copper substrate is even better than copper itself).[11,26] Also, reducing the effective thermal resistance of the entrained gas boundary film between the substrate and the melt (using reduced ambient pressure to vacuum conditions or substituting He for air)[25,27,28] can be very effective in increasing h. While it can be argued that reduced ambient pressure (1) produces a thinner or more dilute boundary layer effectively increasing h, or (2) results in a lower surface count of gas pockets or voids on the contact surface (where the noncontacting void interface may have an associated volume of slower cooled material because of a localized decrease in h values)[25,29] so that the arithmetically averaged value of h does increase in both cases relative to the h value for one atmosphere, it is clear that in either case higher heat transfer rates can be achieved this way. Calculations[30] also show that reducing the substrate temperature to maximize its difference with the solidification temperature is important to insure a high solidification rate and large undercooling effects. This has stimulated the development of a liquid nitrogen cooled rotating substrate subsystem to make and evaluate higher solidification rate melt spun products.[31] The thermal resistance of the already solidified foil between the substrate and the melt can also decrease the average heat transfer rate as the growing thickness of the product becomes greater. Thus for each alloy system that can be melt spun into an amorphous foil, the critical (maximum) thickness at which a fully amorphous cross section can still be produced should be inversely related to the specific alloy dependent minimum cooling rate necessary to retain an amorphous structure during rapid melt quenching. Such correlations have been made with a variety of alloys by using a melt spinning unit with a rapidly braked substrate wheel[16] to produce continuous foils with a graded range of thicknesses; crystalline phases are detected whenever thicknesses exceed the critical thickness that is specific to each alloy composition. Typical values for critical thickness lie in the 100 μm to 150 μm range, but values as high as 225 μm have been measured for alloy systems with very sluggish crystallization kinetics.

While the attainment of melt puddle stability can be linked with the formation of uniform, high quality melt spun product, with few exceptions the principal means of assessing the effects of processing and materials parameters on this dynamic phenomenon have been based on retrospective interpretations of foil product characteristics and/or modelling calculations. Fortunately a few reports where high speed photography has been

used to observe the melt puddle phenomena have been published.[14,19,22,32,34] These generally relate the overall shape and dimensions of the melt puddle with process variables and changing conditions for the easy-to-melt-spin alloy systems that typically form glassy alloy ribbons. In these cases a human foot shaped puddle forms with an upstream heel section ahead of the incoming melt jet and a downstream toe section that tapers down to the final foil thickness. Since foil thickness (t) has been directly related to puddle length (l), it has been possible to increase l by: (1) independently reducing the tangential surface velocity of the substrate,[14,19,32] (2) increasing the jet velocity or mass flow rate,[19,32,33] and (3) using shallower (than 90°) jet/substrate impingement angles.[19,32,34] Limits on many of these process variables are imposed by puddle dynamics. Apparently the puddle can retain its basic shape and absorb minor perturbations as long as the melt spinning system is run within a window of desirable operating conditions. Outside of this range too little spreading (resulting in insufficient solidification through limited heat transfer) or too much spreading (resulting in an extended surface area puddle with undamped instabilities) can lead to the formation of a product with degraded quality characteristics.[14,19,22,32-34]

Methods to externally stabilize the melt puddle have been reported using a controlled introduction of He gas just upstream of the melt puddle[34,35] or coaxially with the melt jet.[36] The intended reduction in fluid turbulences and enhanced cooling effects did result in improved quality products. The use of a mechanical constraint (typically by moving the external surface of the melt ejection nozzle in close proximity with the moving substrate surface)[14,28,32,37,38] has been very successful in reducing the free surface oscillations of the melt puddle and enabled the use of slotted orifices to melt spin wider, high quality foils.

Finally, the least amount is known about the interfacial bond that forms after the melt has wet and then solidified on the rotating melt quenching wheel. However, to assure process continuity this bond must be relatively weak to allow foil/wheel separation prior to one complete revolution. With the exception of one study[24] that specifically compared the effects of wheel surface finish and the resultant contact surface morphology of the foil with the sticking distance (e.g., the puddle to foil/wheel release distance), no other direct information about the nature, geometry, or strength of this foil/substrate interface has been available. In the latter, a geometric argument was used to suggest that the shorter sticking distance for foils with transversely oriented air pockets (produced using a matte surface finish wheel) occurs because these foils can be more

easily broken away from the wheel surface than foils with longitudinal air pockets melt spun off a circumferentially polished wheel surface.

Most other reports provide empirical trends regarding the magnitude of the sticking distance (and by inference the bonding force) as a function of processing factors. In generalized terms, increases in sticking distance can be attributed to a rise in the baseline (lowest) temperature of the substrate wheel[14,36,39] and/or to progressive thermomechanical wheel surface degradation.[14,32,34] Since even the best designed internally cooled melt quenching wheels experience some rise in baseline temperature (the exact magnitude determined by the thermal demand and the thermal efficiency of that subsystem), statements that the sticking distance increases with: (1) running time,[13,14] (2) decreasing wheel diameter, [14,15,36] (3) decreasing thermal conductivity of the wheel material,[14] and (4) increasing product width[14] can be rationalized as consistent with changes in either or both wheel surface conditions.

3. EXPERIMENTAL PRACTICES

3.1 APPROACH

Since various materials and processing parameters can have an interactive impact on the melt spinning phenomenon, a generalized evaluation to identify significant parameters can be quite complex. Our basic approach was to systematically investigate changes in the dynamic phenomenological interaction for a range of melt and substrate materials by initially using an experimental setup where the remaining process variables could be reproduced consistently. Rather than attempting to develop melt spinning procedures and then define "standard" conditions for every material combination, a straightforward testing procedure that simulates the thermal and mass flow conditions of melt spinning was developed. Identifiable characteristics that are significant to this transient, dynamic wetting/solidification interaction would then be used to empirically classify various material (melt/substrate) combinations from these Falling Droplet/Inclined Substrate Plane (FD/ISP) experiments. Next, a more limited group of materials representative of each FD/ISP class will be melt spun. Phenomenological observations, as well as the resultant product features, would then be used to correlate these factors as they relate to processability with the previous results and projections from the FD/ISP test series.

3.2 FALLING DROPLET/INCLINED SUBSTRATE PLANE EXPERIMENTS

The FD/ISP testing procedure has been developed to provide a consistent method for evaluating the dynamic wetting solidification interaction between any desired combination of melt and substrate materials. Essentially, a molten droplet falling a known distance impacts on an inclined substrate to simulate the transient thermal and mass flow conditions of melt spinning (Figure 1). Using high speed cinematography, the wetting behavior and the phenomenological dynamics of this liquid-solid interaction can be recorded and, together with sample analysis, can be used to characterize these experiments.

Each experiment is run in a vacuum (10^{-6} Torr) environment to eliminate ambient gas reactions as well as the gas boundary layer (always attached to the rotating substrate when operating in a gas ambient), both of which could affect to some degree the primary melt/substrate phenomena. Electron beam melting off the end of a standard diameter (typically 0.250 in. in diameter) bar with the desired melt composition that has been locally undercut (typically to a 0.080 in. diameter neck section) at a fixed distance from the free end (typically 0.125 in.) provides a known

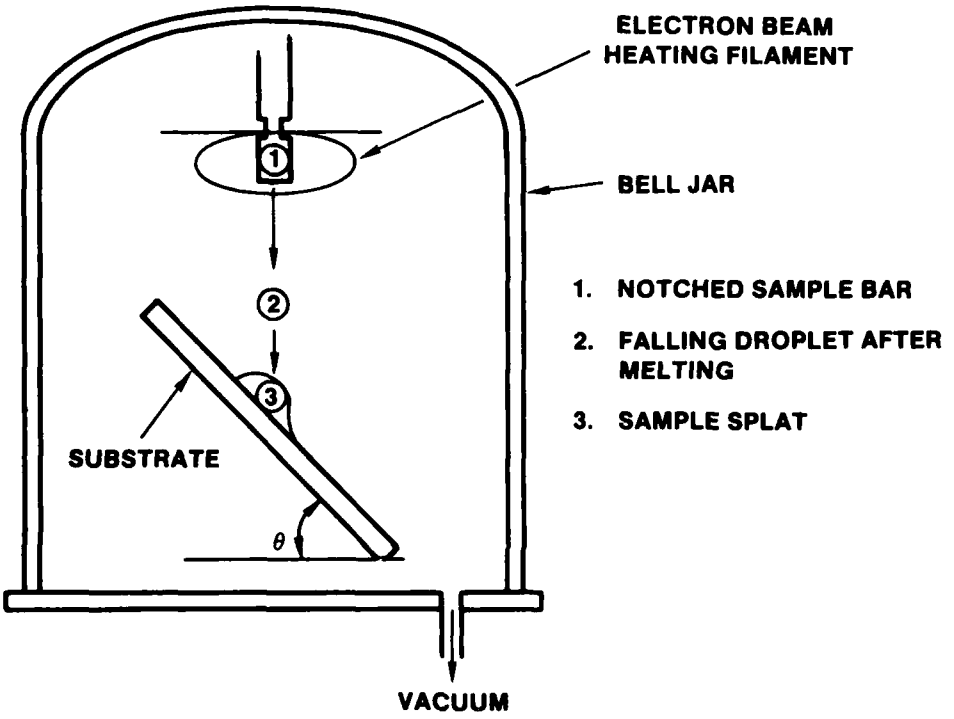

Figure 1. Experimental Setup for Falling Droplet/Inclined Substrate Equipment

volume droplet (typical sphere diameter is 0.23 in.). This crucibless melting method also eliminates preliminary concerns for crucible selection and orifice preparation which may be significant for reactive and/or high melting temperature materials.

The use of small interchangeable substrate plates allows a wide sampling of substrate material and surface finishes as required. Process variables include: (1) initial substrate temperature (with both cryogenic and hot stage temperature control capabilities possible), (2) the droplet falling velocity (calculated at 60 in./s when the standard 4.7 in. drop distance is used), and (3) the substrate inclination angle θ (for changing the relative ratio of the resolved transverse and longitudinal impact forces).

3.3 MELT SPINNING EXPERIMENTS

Free jet, chill block melt spinning experiments were conducted in air to provide more direct information on the nature and dynamics of this complex process as a function of materials and process parameters. Closeup, high speed cinematography provided records of the various phenomena that were occurring in the free jet/melt puddle/substrate region. Complementary sample evaluation also provided a measure of the qualitative and dimensional character of the product from each run.

Typical melt spinning runs started with the inductive premelting of a nominal 50g to 100g charge of the desired composition metal in a capped, melt delivery crucible. Where necessary to prevent oxidation during the heatup cycle, a trickling flow of forming gas (95% N_2-5% H_2) was continually flushed around the charge and through the crucible exiting through the discharge orifice. After melting and upon attaining a nominal 100°C superheat, a preselected forming gas overpressure between one and 5 psi was used to eject the molten charge through a one mm diameter orifice onto the rotating substrate surface. The orifice exit to substrate surface standoff distance was fixed at 0.53 in., allowing easy observation of any unencumbered motion of the resultant melt puddle. The jet was directed with a perpendicular impingement angle (α = 90°) at the top dead center position of the rotating substrate wheel.

For the first series of melt spinning runs the melt quenching subsystem used an 8 in. diameter OFHC Cu wheel. This internally water cooled substrate was rotated at a fixed rate of 1500 rpm (a nominal 600 in./s circumferential surface velocity rate). Continuous surface dressing was provided by a counter rotating flapper wheel device using an abrasive (500 grit) tape media. All other process variables with the exception of

the overpressurization value were deliberately fixed to simplify the analyses.

Typically, the longitudinal profile of the melt puddle was photographed to analyze this dynamic phenomenon for both short- and long-term changes. Head-on views showing the transverse puddle profile were also selectively photographed. At 1000 frames per second it was possible to detect macroscopic changes in the jet and puddle shape. Thus measures of the relative dimensional stability of these phenomena as a function of material and process parameters are possible. In addition the spatial and temporal variation of dynamic wetting can be roughly evaluated.

4. RESULTS AND DISCUSSION

4.1 CHARACTERIZATION OF THE SIMULATED TESTING SYSTEM

In order to demonstrate that useful information about the interacting dynamic wetting and solidification phenomena can be generated using the FD/ISP equipment, evaluation testing started with a group of candidate molten metals that had a wide range of melting temperatures and surface energies (Table 1, where ROM indicates a calculated rule of mixtures value). For this series OFHC copper coupons freshly prepared with 320 grit emery paper to have a reproducible surface finish of 16 μin. CLA were used as a standard substrate. Evaluation of the droplet impact and subsequent solidification phenomena were systematically conducted as a function of substrate inclination angle for five melt compositions. General observations of the impact phenomena and any solidification that occurs were made from high speed motion pictures using a camera aimed directly at the front of the inclined substrate with a horizontal viewing angle. The initial impact and the following spreading phenomena at any given inclination angle were essentially independent of the droplet composition. Each impacting molten metal sphere spreads into an elongated disc due to resolved gravity forces which causes differential flow on the inclined plane. From these filmed records, any increase in the substrate inclination angle was found to promote translational liquid metal flow down the ramp so there is a proportionate decrease in width (the transverse dimension) and increase in length. The nominal maximum width of the still molten disc for all these melts at any given inclination angle fell within a narrow 10% scatter band that was inversely proportional to $\sin\theta$; the extreme values at $\theta = 20°$ and 70° are indicated by the solid dots in Figure 2. This is characteristic of fluid flow conditions where the initial spreading phenomenon is dominated by momentum forces.

Next restoring forces due primarily to surface tension cause different degrees of dimensional retraction and wetting. Only changes in width (the lateral dimension) can be unambiguously measured from film records; a systematic trend was related to inclination angle with magnitude differences separately attributed to composition. Partial retraction with simultaneous solidification results in splat formation while complete retraction is represented by droplet recollection and frequently droplet rebound away from the impact site at high inclination angles. With increasing inclination angle the projected droplet-substrate contact area as well as the resolved substrate surface velocity increases, leading to more pronounced subdivision of the original melt volume. This breakup is caused by the

TABLE 1

COMPARATIVE MELT VALUES

MATERIAL	MELTING TEMP. (°C)	PROPERTIES OF MELT NEAR MELTING POINT SURFACE TENSION (DYNE/CM)	DENSITY (GM/CC)
Zr	1857	1500	5.8
Ni	1455	1780	7.9
80 Ni-20 Cr	1455-1400	1730 (ROM)	7.6 (ROM)
Ni-4.5 Si-2.8 B	1024-966	Less than Ni	Less than Ni
Cu	1083	1300	7.9
Al	660	900	2.5

(ROM): Calculated Rule-of-Mixtures Value

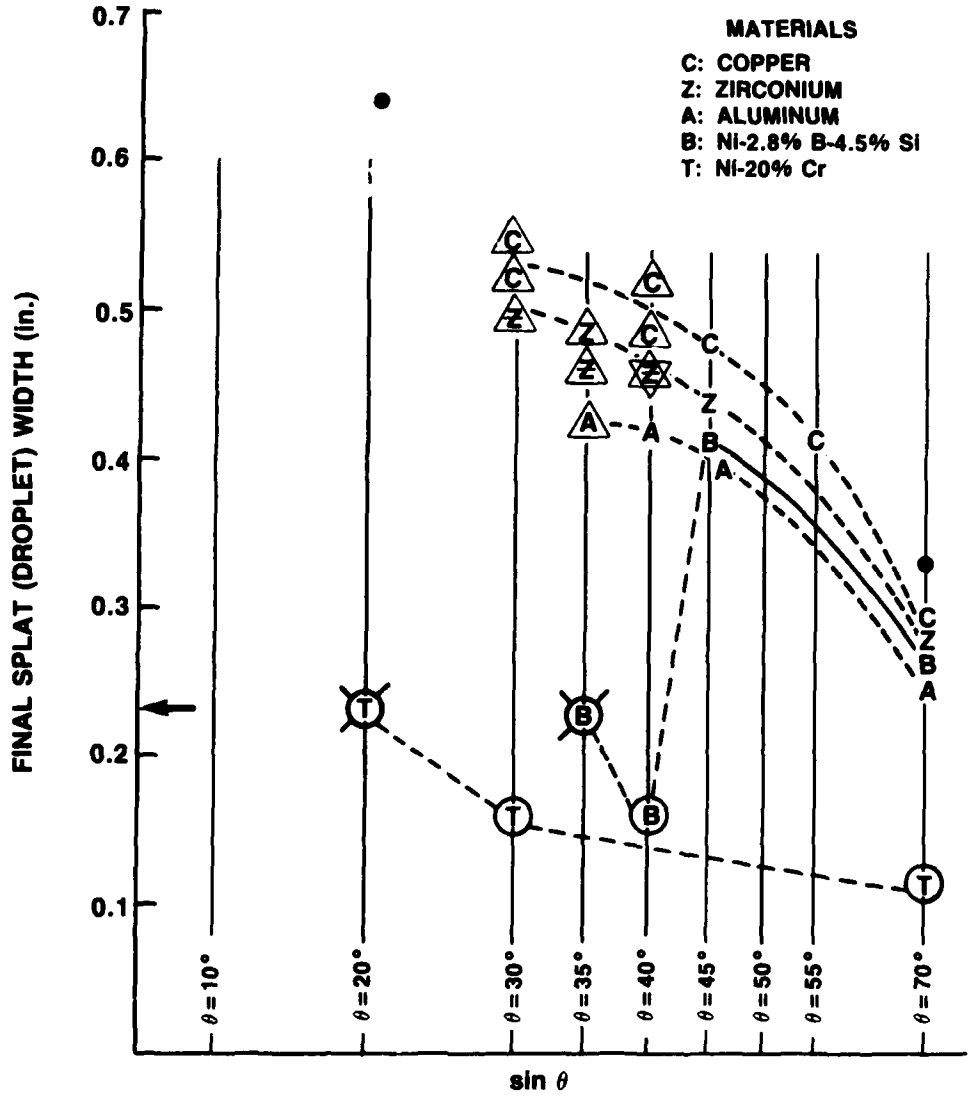

Figure 2. Relationship Between Final Splat Width or Droplet Diameter and Inclination Angle θ

overflow mechanism where the top most region of still hot liquid can rapidly flow over a cooler, more viscous or even solidified lower portion of the melt having more intimate thermal contact with the substrate. Since this relative overflow velocity increases with inclination angle, less original material remains with the primary impact disc resulting in either a smaller volume, primary droplet or splat. More quantitative data and discussion of these systematic trends will be organized and separately presented for each of the two limiting classes of dynamic wetting behavior.

For the nonwetting classification of melt/substrate combinations, the empirical criterion is that post impact droplet reformation must occur. Surface energy reduction is the dominant driving force causing a high retraction rate for the still liquid splat with extended suface area to collapse into a droplet with a minimum surface area to volume ratio. Generally, the apparent absence of wetting indicates that any attractive forces between the liquid (melt) and solid (substrate) phases do not significantly reduce the total surface energy of the system enough to also reduce the retraction rates to levels where droplet reformation is prevented.

The 80% Ni-20% Cr alloy was found to fit this nonwetting category, since on impact with a copper substrate the spreading, recollecting and rebounding process occurred at all inclination angles. The diameters of each primary rebounding droplet decreases with increasing inclination angle. This data is plotted as encircled T symbols as a function of the inclination angle in Figure 2. Also indicated by an arrow is the magnitude of the original pre-impact droplet diameter. Due to the liquid overflow mechanism, the size of the primary droplet diameter decreased with increasing inclination angle. Only for angles of 20° or less was droplet breakup avoided (indicated by the starred T symbol). Freezing of the primary droplet on the substrate near the original impact point was possible only when a 10° inclination angle was used. This near spherical solid form had a minimal substrate contact area with a qualitatively high contact angle such as would be characteristic of a nonwetting sessile drop sample.

For the wetting classification of melt/substrate combinations, the empirical criterion is that during falling droplet testing splat formation and solidification must occur. In this case the spreading drop maintains a rather intimate contact with the underlying substrate after impact, promoting the rapid transfer of heat into the colder substrate. Then any combination of higher fluid viscosity or partial solidification can retard the surface energy driven droplet retraction process and allow the sample to freeze as a solid splat. Examination of wetting features and dimensional patterns on the resultant splat forms can be expected to reveal the effects

of these materials and experimental parameters on the dynamic wetting and solidification phenomena.

Typically Cu, Zr and Al droplets solidify as splats on a Cu substrate, clearly falling into the wetting classification. With increasing inclination angles the tear drop shape (narrow end pointed in the flow direction) becomes narrower and more elongated. The systematic angular as well as metal-to-metal variation of the primary splat dimensions and relative weights are listed in Table 2. Splat width W defined as the maximum lateral dimension, could be reproducibly measured but primary splat length L measurements were more subjective. When melt runnoff was still attached to the primary splat that dimension was labeled total length while primary splat length was gauged from the wetting pattern on the contact surface. Note that only at lower angles does the entire impacting droplet volume get converted to the primary splat (indicated by the 100% values in Table 2 and the triangularly circumscribed data points in Figure 2).

Systematic materials-based differences in dynamic wetting behavior can be empirically discerned from the falling droplet data for Cu, Zr and Al samples. In general the primary Cu splats are wider, longer, and retain a greater percentage of the original droplet material than the comparable array of Al splats while the trend for Zr was intermediate. A consistent, simple explanation for these wetting-type materials with good heat transfer into the substrate could not be made with only one physical property trend listed in Table 1. However, the compound value based on the ratio of surface tension over density could be related to the magnitude of the retarding force. Noting, as discussed previously, that the maximum droplet spreading range is nominally independent of melt composition (when all other experimental factors remain constant), materials systems having larger retracting forces should then have smaller final lateral dimensions. Since the calculated ratios for surface tension over density for Cu and Zr are 46% and 72% of that for Al, the series of final width values for each metal scales well with the proposed inverse relationship for the calculated retraction forces.

Even with solidified splat samples there was little evidence of chemical interaction with or mechanical bonding to the substrate. After cooldown splat samples separated from the substrate without special effort, probably because of differential thermal stresses. These stresses manifest themselves as a slight concave curvature on the contact face of the splat samples. Thus, under these initial conditions foil release should not be a problem. Conditional extrapolations for adequate foil release during melt spinning can also be made if thermal controls and continuous surface dressing practices can retain the original thermal, chemical and morphological characteristics of tne intrinsic wheel surface.

TABLE 2

SYSTEMATIC DIMENSIONAL RELATIONS FOR SOLIDIFIED SPLATS AS A FUNCTION OF INCLINATION ANGLE θ

Primary Splat Width (W) and Footprint Length (L) (Inches); Relative Weight (Percent of Orignal Droplet)

MATERIAL	θ=30° W	L	%	θ=35° W	L	%	θ=40° W	L	%	θ=45° W	L	%	θ=55° W	L	%	θ=70° W	L	%
Copper	0.53	0.68	100%				0.50	0.80 (1.02)*	100%	0.48	0.93 (0.99)*	63%	0.43	1.04 (1.16)*	65%	0.29	1.41	57%
	0.55	0.73	100%				0.52	0.75 (0.90)*	100%									
Zirconium	0.51	0.7	100%	0.49	0.66 (0.81)*	100%	0.46	0.81 (1.08)*	100%	0.45	0.86	53%				0.29	1.28 (1.60)*	46%
				0.48	0.74 (0.95)*	100%	0.48	(0.75) (1.17)*	100%									
Aluminum	PDR		100%	0.42	0.75	100%	0.42	0.65	36%	0.40	0.84	40%				0.24	1.10	26%
Ni-2.8%.B-4.5% Si	DR		100%	PDR		100%	0.45	B	49%	0.42	0.72	55%				0.28	1.11	<50%

Notes: (X)* total length of splat due to attached run-off material.

PDR: partial droplet recollection into non-spherical form.

DR: total droplet recollection and rebound.

B: splat formation with major edge retraction.

Within the general nonwetting class of materials it is expected that surface tension restoring forces should range from dominant to weaker. After impact spreading, dominant force systems will always cause the resultant liquid film to rapidly retract into droplets irrespective of film thickness. For weaker restoring force systems, similar films will not be retracted as rapidly allowing more heat transfer to occur. Thus for a sufficiently thin film, retraction may be impeded or prevented if concurrent solidification occurs. For each melt composition the specific film thickness where this transition first occurs will be inversely proportional to the magnitude of the total surface energy restoring forces. Lower surface energy conditions could result if either the intrinsic surface tension of that liquid is low or if limited or transient melt/solid wetting occurs.

The falling droplet test can be used to qualitatively identify nonwetting systems exhibiting such transitional behavior by empirically establishing the critical inclination angle where splat formation first occurs. Dominant restoring force systems will always display nonwetting droplet retraction pattern even at the highest inclination angles. Weaker restoring force material systems will exhibit a transition from droplet to splat product formation at a specific, critical inclination angle with weaker systems having a lower value for the critical angle.

As previously described, the 80% Ni-20% Cr alloy is a good example of a nonwetting material with dominant surface tension restoring forces. The AMS 4778 brazing alloy (Ni-2.8% B-4.5% Si) on the other hand is an example of a weaker restoring force system with a transitional behavior. As observed in Figure 2, there is the characteristic nonwetting trend at low inclination angles, with a sharp transition to a wetting behavior at inclination angles above 45°. Note also that the location of the plotted curve for the wetting branch behavior of the Ni-2.8% B-4.5% Si alloy is intermediate between the Zr and Al trends. Although the origin of these differences has not been rationalized yet, it is encouraging to point out that this falling droplet test can provide a screening capability for assessing the effects of systematic material and process variations on the dynamic wetting and nonwetting behavior.

4.2 EVALUATION OF DYNAMIC WETTING FOR A SERIES OF Ni-BASE ALLOYS

The dynamic wetting characteristics of a number of model and commercial alloys were investigated in all cases using Ni as the common solvent base. Through the selective choice of solute specie and quantitative content, several alloy classes with different structures as solids

and varying thermophysical properties (e.g., surface tension, viscosity and melting temperature/range) as liquids were evaluated using the falling droplet method.

In addition to the high temperature, oxidation resistant crystalline alloy (80% Ni-20% Cr) and a classic, rapidly solidified amorphous alloy (Ni-2.8% B-4.5% Si), another group consisting of a progressive series of binary Ni-Cu alloys (made at 20% composition intervals) was prepared for this series of dynamic wetting tests. This materials selection rationale allows the evaluation of several melts with regular, but incremental changes in liquid metal properties but where the type of solidification phenomena is essentially the same for all alloys. In particular the isomorphous Ni-Cu binary phase diagram can provide assurances that additional complexities normally introduced when intermetallic phases or two phase solid structures or secondary transformations are involved with solidification will not occur.

A limited number of falling drop tests were run to evaluate the dynamic wetting effects for the Ni-Cu binary series. Only freshly prepared OFHC Cu substrate (given the standard 16 μin. CLA surface finish) were run with 30°, 45° or 70° inclination angles to represent a wide range of impact conditions) for the six melt compositions. Both high speed motion picture observations of the entire interaction phenomenon as well as analysis of the major dimensional measurements (Table 3) confirmed that the entire Ni-Cu binary series behaved similarly to the other wetting class materials over the entire inclination angle range tested. Evidence of limited secondary dimensional variances from sample to sample were noted. Localized peripheral edge scalloping (denoted by "a" in Table 3) or more major edge retraction sections (denoted by "b" in Table 3) were attributed to local sections with lowered heat transfer rates allowing surface tension driven coalescence flow of the residual liquid. For this binary series the insensitivity of the systematic trend of the major dimensional values (especially the widths) as a function of inclination angle to the Ni/Cu ratio was an indication that no critical bulk or surface properties were being changed across the entire alloying range.

Since nominally pure Ni, the Ni-Cu binary alloys, and nominally pure Cu all behave consistently as wetting-type systems, the variations for the other Ni-base alloys must be attributed to some solute specific effect. Additions of Cu are relatively benign. The presence of Cr drastically modifies the phenomenological response of the Ni-20% Cr alloy to the non-wetting case, perhaps due to a residual chrome oxide barrier film. The presence of B (and perhaps Si) may result in the formation of an extremely low surface energy (80 dyne/cm according to Reference 1), self-fluxing

TABLE 3

SYSTEMATIC DIMENSIONAL RELATIONS FOR SOLIDIFIED Ni-Cu BINARY ALLOY SPLATS AS A FUNCTION OF INCLINATION ANGLE θ

Primary Splat Width (W) (Inches)
Footprint Length (L) (Inches)
Relative Weight (Percent of Original Droplet)

BINARY COMPOSITION Cu	Ni	θ=30° W	L	%	θ=45° W	L	%	θ=70° W	L	%
100%	0%	0.50(a)	0.70	100%	0.44	0.82	54%	0.28	1.25 (1.58)*	<57%
					0.42 (b)	0.85 (1.36)*	<100%			
80	20	0.50(a)	0.70	100%	0.4	0.72	40%	0.29	1.43 (2.46)*	<56%
60	40	0.51(b)	0.70	100%	0.43	0.80	56%	(c)	1.60	44%
					0.43	0.85	55%			
40	60	0.50(a)	0.70	100%	0.45	0.86	53%	0.30 (a)	1.50	47%
20	80	0.51(b)	0.66	100%	0.44	0.95 (1.60)*	<100%	0.30	1.20 (1.40)*	44%
								0.31	1.25 (2.67)*	<57%
0	100	0.51(b)	0.70	100%	0.45	0.90	56%	0.30 (b)	1.15	<33%
									(1.60)*	

Notes: (a) localized surface tension driven edge retraction.
(b) major edge retraction.
(c) extreme edge retraction, unable to estimate width.
(x)*total length of splat due to attached runoff material.

liquid boron oxide film that can only be bridged when shearing forces are sufficiently high (e.g., above the critical inclination angle) to produce the transition to wetting behavior. The possibility that an amorphous solidification phenomena promoted by the presence of B could cause the transitional wetting behavior of the Ni-2.8% B-4.5% Si alloy was also considered. However, x-ray diffraction evaluations revealed that all splats were crystalline so that the quench rates for even the thinnest splats were insufficient to retain the amorphous structure. Thus by inference, it is the chemical and not the structural effects of B that produce the transitional dynamic wetting pattern.

To date there is too little information to decide whether the proposed chemical (solute) effects can be related to surface (interface) phenomena or bulk (concentration dependent) alloying effects. Additional data for a variety of substrates and melt phases (with systematic changes in solute concentration) will be necessary to resolve some of these issues. Clearly, it will also be important to make a direct correlation between the dynamic wetting characteristics of material combinations from the falling drop test and the actual melt spinning process characteristics of that same combination of materials. Initial attempts at making these phenomenological connections have been started and will be covered in the next section.

4.3 CHARACTERIZATION OF MELT SPINNING EXPERIMENTS

An initial series of well calibrated, free jet melt spinning runs were conducted on an 8 in. diameter internally cooled OFHC Cu substrate wheel for materials representative of the dynamic wetting class as well as an alloy that exhibits the transitional dynamic wetting behavior. Existing quartz melt delivery vessels were routinely used for two alloys with moderate melting temperatures (Ni-2.8% B-4.5% Si and OFHC copper) without melt/crucible reactivity or thermal stress failure problems. The convenience of using a transparent container to visually monitor the direct inductively coupled charge heatup/melting cycle facilitated progress for this group of alloys. For the higher melting, more reactive Ni-20% Cr alloy as well as the higher Ni content Ni-Cu binary alloys, the use of alumina containers with higher use temperatures that were also chemically resistant to the melt was mandatory. Associated thermal shock sensitivity of alumina requires that an external susceptor heat source be used. The necessary hardware adaptations are being implemented and results will be presented during the next reporting period. In addition, a parallel series of melt spinning experiments with a molybdenum substrate wheel will be also subsequently conducted to evaluate the effects of substrate properties on the process phenomenology.

Each run provided qualitative information about the puddle dynamics and associated wetting/spreading and solidification phenomena for the duration of a run. Careful analysis of high speed motion pictures were used to generate systematic quantitative data against which overall phenomenological behavior as well as product dimensions and quality might be correlated with significant characteristics from the falling droplet experiments. Comparisons with previously reported phenomenological observations from the literature will also be used to augment a better understanding of the phenomena.

To obtain a general understanding of the dynamic wetting/solidification phenomena associated with favorable melt spinning conditions, experiments with the easy-to-melt-spin Ni-2.8% B-4.5% Si brazing alloy melts were conducted. A limited number of melt delivery rates were separately used to produce samples where different characteristics could be attributed to a specific controllable process variable, namely the melt delivery vessel overpressure.

The effect of raising the overpressure is to increase the jet mass flow rate (roughly in proportion to the square root of this overpressure value) and the weight per unit length of solidified fiber. The dimensional values of ribbons formed under these conditions are listed in Table 4. All ribbons had localized free surface undulations but had nominally the same thickness of 0.002 in. as measured with planar tipped micrometers. Since this technique measures the maximum elevation, when surface relief is present a maximum ±20% point to point variation would be much larger than the actual value based on average cross-sectional thickness. Note particularly the far less than 5% variation in the weight per unit length values that represent the average cross-sectional area as well as the relatively constant psuedo value for thickness (based on the ratio of weight per unit length divided by the average foil width); both are good indications that the average cross-sectional thickness is relatively constant along the length of the ribbon.

Thus systematic dimensional accommodations to changes in the rate of liquid metal supply appear mainly as changes in the width of the ribbon product, a secondary longitudinal periodicity in foil width (both in amplitude and frequency of this varicosity effect), and also the quality or character of the finish of the ribbon edge. As a matter of record it can be stated that there was no correlation between the micrometer measured thickness at any longitudinal position including sections with a width maximum or minimum.

Another manifestation of the dynamic balance between jet mass flow rate and product width is the occurrence of periodic width minima and other

TABLE 4

MELT SPUN PRODUCT CHARACTERISTICS (AMS 4778)

Over-Pressure (psi)	Weight Per Unit Length (gm/m)	Foil Width (inches)(c) Average	Max	Min	Min. to Min. Distance (inches)	Comments
5	0.63±0.01(a)	0.080-.120	-	-	highly irregular*	rough edges
2	0.58±0.01(b) and 0.65±0.01	0.070	0.075 -0.080	0.060	1* (semi-irregular)	
1.5	0.57±0.02	0.065	0.070	0.050	4	very short minima sections
1	0.45±0.01	0.045-0.050	0.047-0.052	0.037-0.042	2.5	extended varicosity
1	0.41±0.01	0.045	0.045-0.050	0.025	2	

* amplitude of periodicity is asymmetric with respect to major foil axis

(a) see text to explain low value

(b) anomolously low value attributed to lower melt discharge rate at start of run

(c) measured with low power optical filar scale

edge effects. When the feed rate is well matched with the wheel velocity (e.g., the 1.5 psi run with a 1500 rpm wheel rotation rate) the minima are relatively minor (in length and magnitude) and infrequent (with a larger longitudinal spacing). At lower feed rates (either 1 psi run) the product is not only substantially narrower, but the more extensive and frequent minima indicate that the instantaneous mechanism to accommodate an "insufficient" melt delivery rate is puddle width shrinkage. With increasing overpressures the excess liquid delivery rate causes lateral puddle bulging, producing a wider foil (such as for the 2 psi run) where the amplitude of the width perturbations becomes more asymmetrical and irregularly more frequent. At even higher overpressures (e.g., the 5 psi run) surface tension forces can no longer restrain the bulging puddle, so that excess liquid is transversely shed from the lateral edges of the puddle causing highly irregular edges with slivers and a lower than projected value for the weight per unit length value of the ribbon.

Concurrent high speed motion picture photography provided useful visual images of the complex fluid flow and the melt/gas/substrate interaction phenomena as a function of material and process conditions. For the easy-to-melt-spin Ni-2.8% B-4.5% Si system, the emerging free jet forms an oscillating, human foot shaped puddle over a spatially fixed region where it impacts the rotating substrate surface. With a viewing direction mutually perpendicular to the jet and foil velocity vectors, the longitudinal profile of the puddle was observed and characteristic values were measured (Table 5). A combination of the wheel boundary layer wind and shear forces generated by the rapidly moving substrate surface causes the upstream region (directly under the jet) to form into heel-like shape with an apparent obtuse contact angle (ϕ_u) varying semiperiodically between 110° and 140°. For this section, the additional dynamic (mechanical and fluid flow) forces essentially resists liquid spreading across this continuously advancing interface and shifts the balance between the three surface tension vectors such that this "advancing dynamic" contact angle is probably larger than the intrinsic one from equilibrium sessile drop experiments. The downstream "toe" section is thinner, smoothly flairing into the free surface of the exiting foil with an acute "receding dynamic" contact angle (ϕ_d) between 10° and 30° that is also likely to be less than the intrinsic contact angle, because now the motion favors liquid spreading. No direct quantitative comparison with contact angles estimated from splat edge profile produced during falling droplet testing can be fairly made. However, all the splat contact angles for the transitional and wetting class materials were acute. Thus these dynamic shifts to the intrinsic contact angle $\Delta\phi$, can be estimated to be 50° if the advancing and receeding components are equivalent.

TABLE 5

MELT SPINNING PUDDLE CHARACTERISTICS
(FROM LONGITUDINAL PUDDLE PROJECTION)

Material	Parameter	Melt Spinning Condition P = 1 1/2 psi 1500 rpm	Melt Spinning Condition P = 1 psi 1500 rpm
AMS 4778	Maximum puddle height, H	2.8 ± 0.4 mm	2.4 ± 0.4 mm
	Puddle footprint (melt/substrate contact length, l_c)	3.85 ± 0.6 mm	4.4 ± 0.5 mm
	Projected puddle Area (relative units), A	197 ± 20	201 ± 15
	Variation in projected area, ΔA	± 10%	± 10%
	Contact Angles		
	Øu (upstream)	125 ± 15°	(a)
	Ød (downstream)	20 ± 10°	(a)
OFHC Copper	H	3.4 ± 1.7 mm	3.1 ± 1.5 mm
	l_c	2.6 ± 0.8 mm	2.3 ± 0.7 mm
	ΔA	± 100% (b)	± 100% (b)
	Øu	160 ± 15°	(a)
	Ød	30 ± 20°	(a)

(a) not measured but estimated to be similar to values for 1 1/2 psi

(b) estimated

Measurements of the puddle height, the puddle footprint (or melt/substrate contact) length and the projected area of the longitudinal puddle profile were also made (Table 5). Overall, the projected area of the longitudinal puddle profile was found to remain essentially stable over the entire run that consisted of more than 300 substrate rotations. Localized pseudo-cyclical profile changes are detectable including some short term (under 2×10^{-3}s) heel/wheel liftups. However, the areal values remain nominally constant due to compensating motions around the free and contact surfaces of the puddle periphery. Note also that although the 1½ psi overpressure melt spinning run had a 40% greater mass flow rate than the 1 psi overpressure run, the respective puddle dimensions (height and contact footprint) and projected areas were very similar. Thus as confirmed by ribbon width measurements, it appears that lateral puddle width is primarily controlled by melt delivery rate while longitudinal puddle dimensions are controlled by the balance between shearing (e.g., substrate velocity) and surface tension forces.

In order to gain a better understanding of the transverse puddle behavior of this brazing alloy during melt spinning (at 1 psi overpressure and a 1500 rpm substrate rotation rate) "head on" high speed motion pictures were taken and analyzed. Characteristic data during the first revolution of the substrate wheel and for subsequent steady state conditions are listed in Table 6.

At startup puddle dimensions appear to be more variable as well as larger but these soon reach steady state values for the remainder of the run. The transverse profile below the upper free jet region is usually bulbous in form (with the equitorial or maximum width W_m exceeding the melt/substrate contact width W_c by 10% to 20%). For the rest of the time (up to 25% of the movie frames) the profile is gradually tapered where W_m and W_c can approach each other spatially. Compared to the relatively stable areal values for the longitudinal profile (with a nominal 10% variability), the long term variation in the transverse profile shape and area was estimated to have a factor of two change in area (based on a coupled increase of 20% for W_m and 50% for the puddle height for the largest bulbous forms). These results support the earlier proposal that lateral puddle bulging/collapse accommodates variations in long term changes in mass flow rate and, by inference, local perturbations that appear as periodic necks in the foil width.

The degree of contact between the puddle and the substrate was more difficult to resolve from these transverse photographic records. However, most of the time the bulbous profile has a nonwetting dynamic contact angle

TABLE 6

MELT SPINNING PUDDLE CHARACTERISTICS (FROM "HEAD-ON" VIEW LOOKING DIRECTLY AT EMERGING FOIL)

Parameter	Values During First Revolution	Steady State Values
Average Puddle Height	1.8 ± 0.5 mm	1.5 ± 0.3 mm
Transverse Melt/Substrate Contact Width, W_c	1.76 ± 0.4 mm	1.58 ± 0.25 mm
Variation in Projected Area	± 100% (a)	± 100% (a)
Contact Angle for Transverse Edges, Øe	120 ± 15° (b)	(c)

(a) estimated

(b) Typical value excluding one third of motion picture frames which exhibited one or both contact angles between 90 and 80° but not less than 70°.

(c) Not measured but similar in magnitude and frequency as values during first revolution.

clearly greater than 90° with the cited 120° value subject to some uncertainty due to parallax considerations. Less frequently more dynamic wetting was observed when one or both contact angles had values around 90° or slightly less. For these conditions the puddle had a tapered shape or the bulbous shape was less pronounced or asymmetric; the puddle also often appeared smaller than the average. While this wetting pattern was ambivalent, as expected the transverse contact angle was still intermediate between the extreme values for the upstream and downstream contact angles determined from the longitudinal profile of an equivalent melt spinning run.

It should also be noted that the contact width W_c was consistently larger than the measurements of average foil width (1.2 mm ± 0.2 mm) taken from foil samples. Thus, it must be concluded that while high speed photography of the transverse puddle profile behavior can provide useful information, it has definite limitations in quantitatively resolving puddle/substrate interactions on the microscopic scale.

Experiments with OFHC copper were also conducted to provide immediate comparative information for the melt spinning behavior of that class of materials that had previously been categorized by dynamic droplet testing as having wetting characteristics. All preparatory and experimental conditions as well as equipment parameters (except the nominally 60°C higher melt discharge temperature) were unchanged from those for the previous series of Ni-2.8% B - 4.5% Si alloy runs.

Concern that the potentially greater degree of product/substrate wetting would generally hinder foil release was not an issue for at least the first ten substrate revolutions. However, a sequential buildup of unreleased copper product from one or two highly localized sections on the substrate wheel proved to be highly disruptive. With each revolution the passage of this projection through the puddle, which in and of itself has little inherent stability (as revealed by high speed photography), caused violent oscillations with associated liquid droplet ejection and was also the precursor of a general surface buildup in the form of a semicontinuous copper ring on the substrate. Thus, typically only part of the nominal 100g molten charge was converted to foil before the useful observational phase ended. No specific discontinuities at the deposit/wheel interface were positively identified. However, the absence of an effective site from the very first rotation of each run, as well as a lack of a similar phenomenon for the Ni-base brazing alloy, implies that any bonding agent within the copper product may become more effective as the baseline surface temperature of the substrate rises above room temperature.

The initial foil product was semicontinuous but usually greater in length than the wheel circumference. It was characterized by poor dimensional width and thickness uniformity and could be described as a longitudinally striated/porous film.

Examination of the high speed cinematographic records (quantified in Table 5) shows that the longitudinal profile of the copper melt puddle was highly unstable with psuedo-cyclical temporal fluctuations with substantial changes in volume and shape that are somewhat proportional to the melt delivery rate. No unique shape could be ascribed to the copper puddle; rather, counter-substrate flow of part of the melt seemed to periodically build up the volume of an oscillating liquid pocket that grows to double its height before collapsing into the melt jet and thence cascading onto a very short (by an order of magnitude less than the rear projection) toe or downstream section with accompanying ejection of liquid droplets. Since copper has a considerably shorter footprint length (which essentially reduces solidification times and the growth of thicker, more useful ribbons) and larger upstream and downstream dynamic contact angles than the equivalent values for the Ni-base brazing system, these parameters can be used to signify that less desirable rapid solidification conditions prevail. Substantial process or alloying adjustments clearly will have to be determined to stabilize and modify puddle shape in order to upgrade the quality and reliability of melt spun copper products.

5. CONCLUSIONS

This investigation of the critical dynamics of rapid solidification has used the results of both simulation testing and actual melt spinning experiments to achieve a better understanding of this complex, interactive heat and mass transfer phenomenon. As shown by both testing modes the flow and wetting behavior of a molten metal impacting on a solid surface is strongly influenced by the magnitude and relative direction of any concurrently acting mechanical forces which in turn influence the solidification pattern.

Simulation testing with discrete molten droplets impacting on an inclined substrate plane with systematic variations in inclination angles provided an empirical series of interaction phenomena for each melt substrate combination evaluated, which has been used to classify various forms of transient solidification phenomena. Common to all classes was the similarity of the initial physical spreading process, which is dominated by inertial forces. During this phase the droplet is converted on impact into an elongated disc whose aspect ratio is proportional to the inclination angle. Discs of any material having little tendency to wet a particular substrate also are presented with little opportunity for heat transfer into the substrate so that the still liquid disc will recollect into a droplet(s) with the minimum surface area to volume ratio as driven by strong liquid surface tension forces. Combinations that acted in this fashion were labeled as nonwetting.

As the degree of chemical attraction between the melt and the substrate becomes greater, the resultant interface becomes more intimate with better opportunity for heat transfer and (partial) solidification. Since the interfacial area proportionately increases with the substrate inclination angle (e.g., due both to the increase in the projected cross-sectional area of the droplet on the substrate as well as that caused by the "overflow" mechanism), the absolute amount of heat that can be passed into the substrate increases; accordingly such thinner, higher aspect ratio tear drop shaped splats are more likely to solidify before retraction can be completed. For melt/substrate combinations with higher degrees of chemical attraction or wetting, concurrent solidification may be rapid enough so that the final splat width as a solid is only somewhat less than the maximum transverse spreading dimension of the liquid precursor disc. These widths exhibited a consistent decreasing trend with increasing inclination angle. Each pair of materials that exhibited this solidification behavior was labeled as a wetting combination. Further discrimination between sets of wetting materials was also possible since each set generated a distinct curve within a family of similar curves.

Transitional material combinations with intermediate to lesser degrees of chemical attraction could also be empirically identified. In these cases nonwetting behavior with droplet retraction will occur at lower inclination angles, but there will be a clear transition over a narrow angular range to wetting behavior at all other higher inclination angles when the primary liquid splat becomes sufficiently thin so that solidification can become a retarding agent to effectively oppose droplet recollection. For each materials combination within this transitional class there will be a specific transition angle. Thus systems with a higher relative tendency to remain nonwetting would be characterized by a higher value for this transition angle.

Observations of the melt spinning phenomenon have also been generalized. For any well designed, thermally stable melt spinning facility, an optimal processing window exists within which product uniformity and continuity can be readily maintained. Phenomenologically this occurs whenever an elongated melt puddle forms and exhibits configurational stability. Once established this form of dynamic mass balance appears to be relatively easy to maintain because the operating system is capable of making self-adjustments to long- and short-term perturbations. When the liquid delivery rate is well matched to the foil exit rate (i.e., the peripheral velocity of the rotating substrate) a uniform, constant width foil is produced. A simple decrease in melt delivery rate, holding all other conditions/parameters constant, will be compensated for by a narrowing of the transverse width of the puddle, in turn producing a narrower but essentially similar thickness foil. Correspondingly, increases in melt delivery rate will produce a wider foil, again with no noticeable thickness changes. However, above a certain mass flow value (essentially governed by the maximum heat transfer capability of that particular melt/substrate/equipment combination), excess liquid will be shed either as individual droplets or in the form of sliver decorated foil edges.

Puddle dynamics appear to be a key factor for optimizing melt spin processability. To date two general phenomenological classes of interaction have been observed as the liquid metal supply stream impacts on the rapidly translating substrate. The complex physical spreading and chemical wetting process produces either:

(1) A relatively stable elongated puddle with a regular co-current liquid substrate flow pattern. This allows adequate melt/substrate contact for the continuous solidification of a dimensionally uniform product; or

(2) An unstable, highly irregular puddle having pseudocyclical fluctuations in both volume and shape. This temporal irregularity is due in part to a noticeable amount of counter-current liquid flow, resulting in the growth of an oscillating liquid pocket behind the melt delivery jet that periodically collapses downstream. There is also a distinctly smaller contact footprint between the liquid and the substrate (than the equivalent situation for a stable puddle) resulting in the production of a far less well developed foil product.

Limited results from this and related melt spinning studies indicate that those (frequently boron containing) alloys with modest critical quench rates that are used to make rapidly solidified amorphous products will form the desired, stable puddles on rotating copper substrate wheels. Since our Ni-2.8% B- 4.5% Si alloy belongs to this alloy group, the assumption will be made that, as characterized by simulation testing, alloys with transitional wetting behavior also have an appropriate balance between surface tension and spreading/wetting properties necessary for stabilizing compact puddles. In contrast, during melt spinning of alloys not expected to form amorphous products such as OFHC copper, highly unstable puddles have been observed. In these cases it appears that the balance has been shifted, with more dominant mechanical and spreading/wetting forces causing the formation of an extended surface area puddle with little interfacial contact with the substrate. Further simulation and melt spinning evaluations with other alloy/substrate combinations (including those alloys representative of the totally nonwetting class and the use of molybdenum substrates) have been planned to expand our experimental data base in order to confirm and generalize these preliminary conclusions.

In summary, the falling droplet simulation testing procedure has the ability to resolve differences in transient rapid solidification behavior for various combinations of materials. These behavioral patterns were associated with free and interfacial surface sensitive conditions that control the resultant heat and mass flow. Since analogous factors can influence the continuous rapid solidification phenomena that occur during melt spinning, the screening potential of this falling droplet procedure looks promising. However, additional experimental data is still required to provide a more rigorous verification of the proposed correlations. Once accomplished this approach could be used to identify promising as well as eliminate undesirable melt/substrate combinations for other process development programs. To date our experience suggests that the better materials combinations are those that exhibit transitional falling droplet wetting behavior where retractive and restraining factors are appropriately balanced to promote desirable melt spinning conditions.

6. REFERENCES

1. A. Bondi, "The Spreading of Liquid Metals on Solid Surfaces," Chemical Reviews 52, 417-445 (1953).

2. R.J. Klein Wassink, "Wetting of Solid-Metal Surfaces by Molten Metals," J. Institute of Metals 95, 38-43 (1967).

3. J.V. Naidich and J.N. Chuvashov, "Wettability and Contact Interaction of Gallium-Containing Melts with Non-Metallic Solids," J. Mat. Sci. 18, 2071-2080 (1983).

4. S.J. Hitchcock, N.T. Carroll and M.G. Nicholas, "Some Effects of Substrate Roughness on Wettability," J. Mat. Sci. 16, 714-732 (1981).

5. J.F. Oliver and S.G. Mason, "Liquid Spreading on Rough Metal Surfaces," J. Mat. Sci. 15, 431-437 (1980).

6. R.S. Timsit, "The True Area of Contact at a Liquid-Solid Interface," Appl. Phys. Lett. 40 [5], 379-381 (1982).

7. N.K. Batra, J.B. See and T.B. King, "Flow Behavior of Liquid Metals on Solid Substrates," Metal Sci., 145-151 (1977).

8. D.E. Polk and D. Turnbull, "Flow of Melt and Glass Forms of Metallic Alloys," Acta Metallurgica 20, 493-498 (1972).

9. C.A. Williams and H. Jones, "The Effect of Melt Superheat and Impact Velocity on Splat Thickness," Mat. Sci. Eng. 19, 293-297 (1975).

10. F.E. Luborsky and H.H. Liebermann, "*Effect of Melt Temperature on Some* Properties of $Fe_{80.5}B_{15}Si_4C_{0.5}$ and $Fe_{40}Ni_{40}B_{20}$ Amorphous Alloys," Mat. Sci Eng. 49, 257-261 (1981).

11. D.M. Kroeger, W.A. Coghlan, D.S. Easton, C.C. Koch and J.D. Scarborough, "A Study of Cooling Rates During Metallic Glass Formation in a Hammer and Anvil Apparatus," J. Appl. Phys. 3, 1445-1453 (1982).

12. K. Togano, H. Kumakura and K. Tachikawa, "Formation of Amorphous Superconducting Transition-Metal Alloys by Liquid Quenching on Hot Substrates," Appl. Phys. Lett. 40 [1], 84-86 (1982).

13. H.H. Liebermann, "The Dependence of the Geometry of Glassy Alloy Ribbons on the Chill Block Melt-Spinning Process Parameters," Mat. Sci. Eng. 43, 203-210 (1980).

14. H.R. Hilzinger and S. Hock, "Preparation of Metallic Glasses," Proc. Conf. on Metallic Glasses: Science and Technology, Vol. I, 71-90, C. Hargitai, I. Bakonyi and T. Kemeny, Eds., Central Research Institute for Physics, Budapest (1980).

15. F.E. Luborsky, H.H. Liebermann and J.L. Walter, "The Effect of Ribbon Thickness, Composition and Process Changes on the Properties of Rapidly Quenched Metal-Metalloid Alloys," Proc. Conf. on Metallic Glasses: Science and Technology, Vol. I, 203-211, C. Hargitai, I. Bakonyi and T. Kemeny, Eds., Central Research Institute for Physics, Budapest (1980).

16. M. Hagiwara, A. Inone and T. Masumota, "The Critical Thickness for the Formation of Ni-Si-B Amorphous Alloys," Met. Trans. 12A, 1027-1031 (1981).

17. D.C. Agrawal, "Melt Spinning Parameters and the Geometry of Metallic Glass Ribbon," J. Mat. Sci. Lett. 1, 385-386 (1982).

18. J.H. Vincent, J.G. Herbertson and H.A. Davies, "Comments on the Geometry of Melt Spin Ribbon," J. Mat. Sci. Lett. 2, 88-90 (1983).

19. H. Hillman and H.R. Hilzinger, "On the Formation of Amorphous Ribbons by the Melt Spin Techniques," Rapidly Quenched Materials III, Proc. 3rd International Conf. on Rapidly Quenched Metals, Vol. I, 22-29, B. Cantor, Ed., The Metals Society, (July 1978).

20. U. Köster, U. Herold and H-G Hillenbrand, "Influence of Solidification Parameters on Mechanical Properties and Thermal Stability of Fe-Ni-B Metallic Glasses," Scripta Metallurgica 17, 867-872 (1983).

21. S.J.B. Charter, D.R. Mooney, R. Cheese and B. Canto. "Melt Spinning of Crystalline Alloys," J. Mat. Sci. Lett. 15, 2658-2661 (1980).

22. H.H. Liebermann, "Gas Boundary Layer Effects in Processing Glassy Alloy Ribbons," Rapidly Quenched Material III, Proc. 3rd International Conf. on Rapidly Quenched Metals, Vol. I, 34-40, B. Cantor, Ed., The Metals Society, (July 1978).

23. C.E. Mobley, R.E. Maringer and L. Dillinger, "Surface Features of Rapidly Quenched Filaments," Proc. International Conf. on Rapid Solidification Processing: Principles and Technologies, 223-229, R. Mehrabian, B.H. Kear and M. Cohen, Eds, Claitors Press, Baton Rouge, LA (1977).

24. S-C Huang and H.C. Fiedler, "Effects of Wheel Surface Conditions on the Casting of Amorphous Metal Ribbons," Met. Trans. 12A, 1107-111 (1981).

25. M. Matsuura, M. Kikuchi, M. Yagi and K. Suzuki, "Effect of Ambient Gases on Surface Profile and Related Properties of Amorphous Alloy Ribbons Fabricated by Melt Spinning," Jap. J. Appl. Phys. 19 [9], 1781-1787 (1980).

26. H. Jones, "Observations on a Structural Transition in Aluminium Alloys Hardened by Rapid Solidification," Mat. Sci. Eng. 5, 1-18 (1969/1970).

27. S.C. Hsu, Internal GTE Laboratories communication.

28. T.R. Anthony and H.E. Cline, "Dimensional Variations in Newtonian Quenched Metal Ribbons Formed by Melt Spinning and Melt Extraction," J. Appl. Phys. 50 [1], 245-254 (1979).

29. J.V. Wood and R.W.K. Honeycombe, "The Structure of Splat-Cooled Fe-20% Cr-25% Ni Austentic Steel," J. Mat. Sci. 9, 1183-1188 (1974).

30. P.H. Shingu and R. Ozaki, "Solidification Rate in Rapid Conduction Cooling," Met. Trans. 6A, 33-37 (1975).

31. D. Pavuna and D. Hainsworth, "A Low Temperature Melt-Spinning Device," J. Noncrystalline Solids 37, 417-422 (1980).

32. H.H. Liebermann, "Manufacture of Amorphous Alloy Ribbons," IEEE Trans. of Magnetics Mag-15 [6], 1393-1397 (1979).

33. J.L. Walter, "A Study of the Formation of Amorphous Ribbon Using High-Speed Motion Pictures," Rapidly Quenched Materials III, Proc. 3rd International Conf. on Rapidly Quenched Metals, Vol. I, 30-33, B. Cantor, Ed., The Metals Society, Vol. I, 30-33 (July 3-7, 1978).

34. D. Pavuna, "Production of Metallic Glass Ribbons by the Chill-Block Melt-Spinning Technique in Stabilized Laboratory Conditions," J. Mat. Sci. 16, 2419-2433 (1981).

35. D. Pavuna, "On the Improvements of Metallic Glass Ribbons Geometry -- the Quenching Stabilizer," J. Noncrystalline Solids 37, 133-137 (1980).

36. H.H. Liebermann, "Coaxial Jet Melt-Spinning of Glassy Alloy Ribbons," J. Mat. Sci. 15, 2771-2776 (1981).

37. M.C. Narasimhan, U.S. Patent No. 4,142,571, "Continuous Casting Method for Metallic Strips" (March 1979).

38. H.R. Hilzinger, K. Krueger and S. Hock, U.S. Patent No. 4,386,648, "Method and Device for Manufacturing Amorphous Metal Tapes" (June 1983).

39. S.R. Robertson, T.J. Gorsuch and R.P.I. Adler, "Advanced Melt Extraction Technology," Proc. International Conf. on Rapid Solidification Processing Principles and Technologies, 188-207, R.H. Mehrabian, B.H. Kear and M. Cohen, Eds., Claitors Press, Baton Rouge, LA (1977).